# Finite-Difference Analysis of Stresses of a Non-Uniform FGM Circular Disk Rotating in Magneto-Thermal Environment: An Equal Mass Study

Pranta Rahman Sarkar[1,*], Akm Samsur Rahman[2]

[1]Department of Mechanical Engineering, Bangladesh University of Engineering and Technology, Dhaka 1000, BGD.

[2]Mechanical Engineering, New York City College of Technology, Brooklyn, NY 11201

Email: sarkarpranta11@gmail.com (PR Sarkar)*

asrahman@citytech.cuny.edu (AS Rahman)

[*] Corresponding author

## A B S T R A C T

The stress field of a functionally graded material (FGM) rotating disk is studied for different cases of non-uniform thickness variation in the magneto-thermal environment. Three different cases of thickness variation are considered by assuming the variation of non-uniform thickness profiles to be linear, rational, and exponential functions of radius. The mass of the FGM disk is considered equal in all cases of uniform/non-uniform thickness variation. The finite-difference method is used to obtain the numerical results for an $Al/Al_2O_3$ FGM disk of fixed-free boundary conditions. The resultant thermo-elastic analysis has shown that the decrease in outer end thickness significantly increases circumferential stress at that end. In absence of magnetic field, for the disk with thin outer end thickness minimum stress intensity can be found with linearly varying thickness profile, and high intensity of circumferential stress in case rational and exponential variation of thickness profiles can significantly be reduced with an optimum magnetic field. The transient stress fields and effect of material properties are also analyzed in detail. All the analyses showed that along with affecting the magnitude, the presence of the magnetic field changes the location and nature of maximum stress in the disk. Finally, results are compared with finite-element method (FEM) and available analytical results to verify the analysis.

***Keywords*:** Numerical solution; Rotating disk; Magneto-thermo-elasticity; Non-uniform thickness; Functionally graded material.

## 1. Introduction

Functionally graded materials (FGMs) represent a group of structural composites in which two or more materials are integrated to meet the desirable properties in any particular application. Due to excellent response in thermal and mechanical loading, the use of functionally graded materials is increasing rapidly in engineering structures. FGMs are mainly suited to the structure which is subjected to a high thermal gradient. In FGMs, material properties can be varied from one surface to another surface in a way that facilitated the reduction in thermal stress in the material transition region. Generally, an FGM structure constructed with metal and ceramics can be used as thermal insulation material. The low thermal expansion coefficient of ceramics also makes FGM structures more suitable for thermoelastic applications. Analysis of various structural components of functionally graded materials is quite extensive in literature [1–10].

The ample use of circular disks in engineering structures inspired researchers to analyze FGM circular disks under different loading conditions. Recently, so many works relating to the stress analysis of FGM circular disks under thermal, magneto-thermal, hygrothermal, etc. loading conditions have been reported in literature. Zenkour [11] analytically solved the elastic behavior of a rotating functionally graded annular disk for four different boundary conditions and exponentially varying material properties. The effect of non-uniform thickness variation on the elastic response of FGM disk has been investigated out by Bayat et al. [12]; they reported that comparing to a uniform disk, an FGM disk with non-uniform parabolic concave or hyperbolic convergent thickness variations are more efficient. Zenkour [13] demonstrated the thermoelastic response of a uniformly thick FGM disk analyzing the effect of angular speed, temperature load, and material properties on the displacement and stress components of the disk. In another analytical study, Dai and Dai [14] solved the thermoelastic behavior of non-uniform FGM rotating

disk under angular acceleration and showed that circular disk with thick inner surface and a thin outer surface, displacement and stresses can be minimized. The thermo-elastic field where material properties are temperature-dependent was analytically studied by Bayat et al. [15] for both uniform and non-uniform FGM disks. An exact solution of non-uniform FGM disk showing the effect of grading index with geometrical non-uniformity on the magneto-thermo-elastic environment was reported in [16]. The magneto-thermo-elastic behavior of a functionally graded uniform sandwich disk showing the effect on the presence of the magnetic field is presented in an analytical attempt by Zenkour [17] under steady-state thermal load.

Side by side with analytical approach, various computational schemes have also been adopted to analyze the multi-physics loading response of FGM circular disks, cylinders, spheres, and other structural components. Zheng et al. [18] used the finite-difference method (FDM) to analyze the elastic field of FGM circular disk and showed that the decrease in outer end thickness and for rationally varying thickness profile, the stress intensity of the disk gets minimum. The finite-difference solution of elastic field of an FG fiber-reinforced non-uniform circular disk rotating with angular deceleration is presented by Zheng et al. [19]. FDM is also adopted by Eldeeb et al. [20] to analyze the thermo-elastic behavior of multilayered FGM disk of non-uniform thickness. Dai et al. [21] implemented finite-difference method to solve the hygrothermal field of functionally graded piezoelectric material circular disk with exponentially varying material properties. The non-linear bending analysis of non-uniform FGM disk combining the dynamic relaxation method with novel finite-difference method is shown in Ref. [22]. Recently, Sarkar and Rahman [23] investigated the thermoelastic behavior of a non-uniform FGM rotating disk in the presence of a magnetic field using the novel finite-difference method (FDM). Their study showed the advantages of FDM in managing non-uniform thickness profile and material distribution for both steady-state

and transient thermal load. Afsar and Go [24] used finite-element method to analyze the thermo-elastic field of a uniform FGM rotating disk; they analyzed the thermoelastic reaction of the disk for different distributions of temperature field and exponentially varying material properties. Leu and Chien [25] implemented the finite-element formulation for FGM disk with variable thickness under non-uniformly distributed heat source and power-law distribution of material properties. Finite-element analysis of composite plate with sector geometry under thermomechanical loading is shown by Shaterzadeh et al. [26]. They studied the response of a plate sector with one or two holes subjcted to a uniform temperature raise in presence of compressive mechanical loading in axial, circumferential, and biaxial directions. Hassani et al. [27] followed three different approaches, namely, variable material properties (VMP), Runge-Kutta's (RK), and finite element (FE) method, to solve the thermoelastic problems of an FGM rotating disk with variable thickness; the correspondence among these solutions are also analyzed in the study. Their analysis has found that in coarser mesh, RK method provides more accurate analysis than VMP, however VMP is easier to implement ensuring less computational effort and memory. Bahrami Babamiri et al. [28] applied first-order shear deformation theory to analyze the effect of geometrical imperfection on the thermo-mechanical bending behavior of rotating FGM disks with temperature-dependent material properties. Coevolutionary particle swarm optimization approach integrating with differential quadrature method is used by Khorsand and Tang [29] to design FGM disk with non-uniform thickness optimizing the weight rotating in thermal environment. Fredholm integral-based analytical approaches are adopted by Peng and Li [30] to analyze the thermoelastic characteristics of FGM circular disk. Deka et al. [31] implemented homotopy perturbation method to analyze the thermoelastic behavior of FGM circular disk with both Dirichlet and Neumann boundary conditions.

Several works have been reported on the transient thermo-elastic behavior of FGM circular disks, cylinders, and spheres. The unsteady-state thermal stress analysis of three-dimensional three-layered annular disk of copper, zinc, and aluminum is made in [32]. The time-varying thermo-elastic reaction of multilayered FGM circular disk was analyzed by Ootao and Tanigawa [33] and found that multilayered FGM model helps minimizing thermal stress compared to the single-layered FGM model. Khorsand and Tang [29] analyzed the transient thermal shock resistance of FGM disk taking the distribution of material properties vary both in radial as well as circumferential direction of the disk. Creep analysis of FGM cylindrical pressure vessels is made by Nejad and Kashkoli [34] showing the effect of the material gradient index with time. A finite-difference solution on the transient magneto-thermo-elastic reaction of cylinder with non-homogeneous material properties is shown by Abd-EI-Salam et al. [35]. The time-varying thermal stress distribution in an FGM sphere with an internal heat source was analyzed numerically by Pawer et al. [36]. They studied the effect of non-uniform heat generation on temperature and stress distributions of the sphere.

Circular disks are extensively been used in rotating mechanisms like circular cutters, turbine rotors, internal combustion engine propellers, high speed gears, flywheels, grinding wheels, computer hard drives, etc. In these practical applications, the rotating disk generally experiences high-temperature variations, and the presence of thermal load significantly influences the deformation as well as stress fields of the disk. Moreover, magnetic field is also found to play a significant role in the displacement and stress fields of an FGM disk; high-stress concentration raised from the presence of thermal load can be optimized in presence of a magnetic field [16,23]. Therefore, a reliable and accurate analysis of coupled multi-physics problems e.g. thermo-elastic, magneto-thermo-elastic fields of FGM circular disk is of utmost importance. Along with

multiphysics loading conditions, non-uniform thickness profile is another important geometrical shape parameter that determines the overall deformation and stress distribution on the non-uniform disk. The high stress intensity in the case of an uniform disk can significantly be reduced by properly selecting the non-uniform thickness profile [18]. But most of the studies on non-uniform FGM disk considered non-uniform thickness variation to be power-law function of radius. However, hardly any literature reported the effect of non-uniform thickness variation on the magneto-thermo-elastic behavior of an FGM disk under both steady-state and transient thermal loading, where the mass of all uniform and non-uniform disks are kept equal. [12,18] investigated the stress field of functionally graded rotating disk where the mass is kept equal in all uniform and non-uniform disk cases. But both works are limited up to the single physics elastic analysis of the rotating FGM disk. Considering the extensive practical applications of FGM circular disk, detailed analysis on the effect of non-uniform thickness profile under coupled multiphysics loading conditions is of great importance to design non-uniform circular disks while increasing their fatigue life cycle by optimizing high stress intensity.

In this paper, we extended the studies of [18,23] with the focus of stress-field analysis of a FGM rotating disk for different cases of non-uniform variation of thickness profile in magneto-thermal environment. Three different cases of thickness profile variation are taken into consideration while the mass of the uniform/non-uniform rotating disk is kept equal in all cases. The temperature fields, as well as the stress fields, are calculated using FDM. Steady-state, as well as transient cases of temperature fields, are considered in this study. Numerical results are investigated for a rotating $Al/Al_2O_3$ FGM disk with fixed-free boundary conditions at the inner and outer surface of the disk, respectively. Initially, the effect of different cases of non-uniform thickness profile on stress components is analyzed in absence of the magnetic field. Later, the effect of magnetic field on

different cases of thickness profile is plotted in a comparative fashion. The distribution of stress fields with time and the effect of material properties on the rotating FGM disk are also analyzed. The validity of the present solutions are also performed by comparing with conventional finite-element method (FEM) and available analytical solution.

## 2. Formulation of the Problem

Figure 1 shows the structural model of an FGM circular disk with non-uniform thickness assuming that the center of the disk is located at the origin of polar coordinate system ($r, \theta, z$). The inner and outer end radius of the non-uniform disk are assigned as, $a$ and $b$, respectively. The dark color in Figure 1a represents material $A$ (at $r = a$) and white colors represent material $B$ (at $r = b$) of the FGM disk. Variation of thickness profile as a function of disk radius is shown in Figure 1b. The disk is considered rotating with a constant angular velocity, $\omega$ in the clockwise direction. The presence of a steady-state magnetic field is also considered in the axial direction ($0, 0, H_0$) of the disk. A uniformly distributed heat source is assumed to be present with allowing out-of-plane convective heat flux from the non-uniform surfaces of the disk, when the inner end ($r = a$) and the outer end ($r = b$) are at a fixed temperature, $T_a$ and $T_b$, respectively. Both the exponential and power-law distribution of material properties are considered for the analysis.

Material properties following the exponential law (E-FGM) in the radial direction as [23,24]

$$M(r) = M_0 e^{n_m r}, \tag{1a}$$

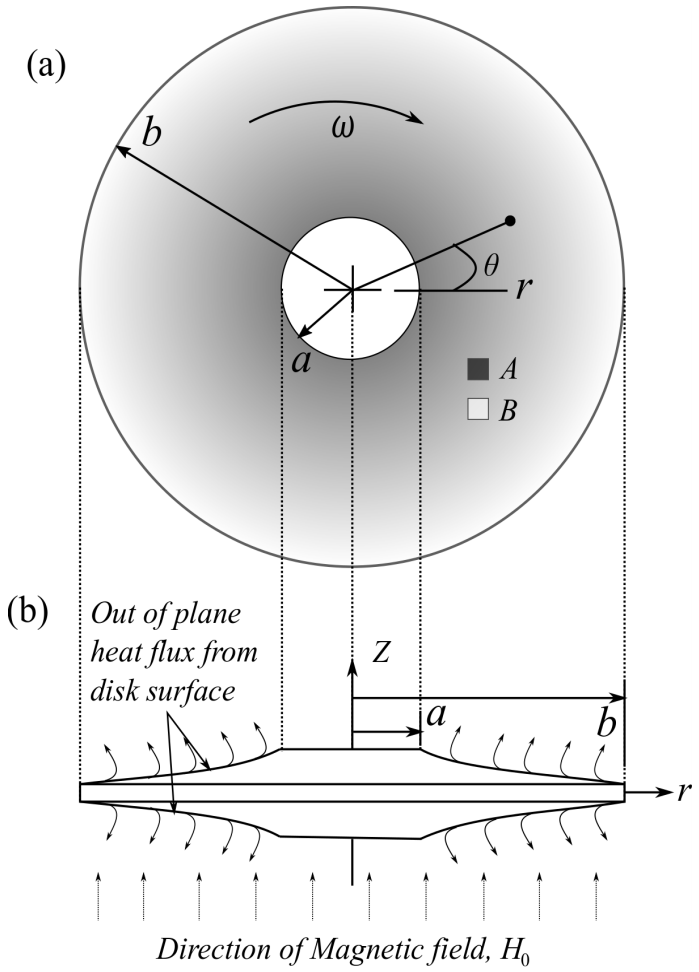


**Figure 1.** Structural model showing the non-uniform thickness variation and loading conditions of the disk.

Where,

$$M_0 = M_A e^{-n_m a} \quad when, n_m = \frac{1}{a-b} ln\left(\frac{M_A}{M_B}\right). \tag{1b}$$

Material properties following the power-law (P-FGM) of distribution as [37]

$$M(r) = M_1 + M_2 r^n, \tag{2a}$$

Where,

$$M_1 = \frac{M_B a^n - M_A b^n}{a^n - b^n} \quad and \quad M_2 = \frac{M_A - M_B}{a^n - b^n}. \tag{2b}$$

Here, $M_0$, $M_1$, $M_2$, and $n_m$ are the unknown constants related to material properties, obtained from the properties of material given at inner end, $M_A$, and outer end, $M_B$. The power-law index of material properties is assigned as, $n$. In this paper, $E(r)$, $\alpha(r)$, $\rho(r)$, $K(r)$, and $C_p(r)$ are considered to be a function of the radius, when $\eta$ and $\mu$ are considered to be constant throughout the disk.

The variation of properties of material is assumed to be only in the radial direction, but the material properties at any point are considered to be identical at all the directions, which makes the FGM disk axisymmetric, and for small thickness variation of the non-uniform disk the present analysis in this paper is made in plane stress conditions.

The fixed-free boundary conditions of the FGM disk at inner and outer ends, respectively, can be expressed as:

1. At the inner end, $r = a$: radial displacement, $u = 0$
2. At the outer end, $r = b$: radial stress, $\sigma_r = 0$

## 3. Modeling of Magneto-Thermo-Elastic Fields

### 3.1. Formulation of magneto-thermo-elastic fields

In a polar coordinate system, under axisymmetric condition, the dynamic equation of equilibrium of a non-uniform FGM circular disk rotating in a uniform magnetic field in (0, 0, $H_0$) direction is [16]

$$\frac{1}{h(r)}\left\{\frac{dh(r)}{dr}\right\}\sigma_r + \frac{d\sigma_r}{dr} + \frac{\sigma_r - \sigma_\theta}{r} + \frac{d\tau_r}{dr} + \rho(r)\omega^2 r = 0. \tag{3}$$

With general strain-displacement relationship, the stress components of a functionally graded material disk in plane stress condition for thermo-mechanical loading is [23]:

$$\sigma_r = \quad P_{11}(r)\frac{du}{dr} + P_{12}(r)\frac{u}{r} - D(r)\Delta T, \tag{4a}$$

$$\sigma_\theta = P_{12}(r)\frac{du}{dr} + P_{11}(r)\frac{u}{r} - D(r)\Delta T, \tag{4b}$$

Where, $P_{11}(r) = \frac{E(r)}{1-\mu^2}$; $P_{12}(r) = \frac{\mu E(r)}{1-\mu^2}$; $D(r) = \frac{E(r)\alpha(r)}{1-\mu}$; $\Delta T = T(r) - T_0$.

Maxwell's electromagnetic stress component, $\tau_r$ in terms of radial displacement [17]

$$\tau_r = \eta H_0^2 \left(\frac{du}{dr} + \frac{u}{r}\right). \tag{4c}$$

Now, substituting the expressions of Eqs. (4) into Eq. (3) for uniform $\mu$ and $\eta$, we will get [23]:

$$(P_{11} + \eta H_0^2)\frac{\partial^2 u}{\partial r^2} + \left\{\frac{P_{11}}{h}\frac{\partial h}{\partial r} + \frac{dP_{11}}{dr} + \frac{P_{11}}{r} + \frac{\eta H_0^2}{r}\right\}\frac{\partial u}{\partial r} + \left\{\frac{P_{12}}{rh}\frac{\partial h}{\partial r} + \frac{1}{r}\left(\frac{dP_{12}}{dr}\right) - \frac{P_{11}}{r^2} - \frac{\eta H_0^2}{r^2}\right\}u$$
$$= \left\{\frac{D}{h}\left(\frac{dh}{dr}\right) + \frac{dD}{dr}\right\}\Delta T + D\frac{\partial T}{\partial r} - \rho\omega^2 r. \tag{5}$$

Eq. (5) is the associate governing equation of a non-uniform FGM circular disk rotating in the magneto-thermal environment. Now, solving Eq. (5) with associated boundary conditions, the displacement field of the disk can easily be obtained.

### 3.2. Solution of governing equation and boundary conditions

In this paper, the finite-difference method (FDM) is implemented to solve the governing equation, as well as the associate condition in the boundaries. To obtain the finite difference solution, the radius of the non-uniform disk is uniformly divided into *N* number of nodes, so, the size of each mesh is, $\Delta r = (b\text{-}a)/(N\text{-}1)$. It should be mentioned here that in the present analysis the local truncation error order is kept equal for all the finite-difference equations formulated both in governing equations as well as in the associate boundary conditions, which is, $O(\Delta r^2)$. The governing equation is discretized by adopting the central difference formulae. Thus, the corresponding finite-difference form of Eq. (5) can be written as [23]:

$$\left[\frac{P_{11}(i)+\eta H_0^2}{\Delta r^2}+\left\{\frac{P_{11}(i)}{h(i)}\left(\frac{h(i+1)-h(i-1)}{2\Delta r}\right)+\frac{P_{11}(i+1)-P_{11}(i-1)}{2\Delta r}+\frac{P_{11}(i)}{r(i)}\right.\right.$$

$$\left.\left.+\frac{\eta H_0^2}{r(i)}\right\}\frac{1}{2\Delta r}\right]u(i+1)$$

$$-\left[\frac{2(P_{11}(i)+\eta H_0^2)}{\Delta r^2}-\frac{P_{12}(i)}{r(i)h(i)}\left\{\frac{h(i+1)-h(i-1)}{2\Delta r}\right\}\right.$$

$$\left.-\frac{P_{12}(i+1)-P_{12}(i-1)}{(2\Delta r)r(i)}+\frac{P_{11}(i)+\eta H_0^2}{r^2(i)}\right]u(i)$$

$$+\left[\frac{P_{11}(i)+\eta H_0^2}{\Delta r^2}\right.$$

$$-\left\{\frac{P_{11}(i)}{h(i)}\left(\frac{h(i+1)-h(i-1)}{2\Delta r}\right)+\frac{P_{11}(i+1)-P_{11}(i-1)}{2\Delta r}\right.$$

$$\left.\left.+\frac{P_{11}(i)+\eta H_0^2}{r(i)}\right\}\frac{1}{2\Delta r}\right]u(i-1)$$

$$=\left[\frac{D(i)}{h(i)}\left\{\frac{h(i+1)-h(i-1)}{2\Delta r}\right\}+\frac{D(i+1)-D(i-1)}{2\Delta r}\right]\{T(i)-T_0\}$$

$$+\left\{\frac{D(i)}{2\Delta r}\right\}\{T(i+1)-T(i-1)\}-\rho(i)\omega^2 r(i). \qquad (6)$$

Here, $i$ ($i$ = 1,2,3…$N$) indicate number of nodes. At the inner nodes ($i$ = 2: $N$-1) of the disk radius, the displacement field can be obtained using Eq. (6). This finite-difference equation can be used with any distribution material properties, as well as non-uniform thickness variations, for both steady-state and transient thermal loading conditions.

Now, for managing boundary conditions, three points forward as well as backward difference formulae are implemented when the local truncation of error is kept in the order of, $O(\Delta r^2)$. At the inner end ($i$ =1) forward difference and at outer ($i$ = $N$) end of the disk backward difference formulae is implemented, respectively. At inner nodes ($i$ = 2: $N$-1) of the disk to obtain stress

components central difference formulae are adopted. The finite-difference expressions of stress components using the central difference formulae are [23]:

$$\sigma_r(i) = \left\{\frac{P_{11}(i)}{2\Delta r}\right\}u(i+1) + \left\{\frac{P_{12}(i)}{r(i)}\right\}u(i) - \left\{\frac{P_{11}(i)}{2\Delta r}\right\}u(i-1) - D(i)\{T(i) - T_0\}, \quad (7a)$$

$$\sigma_\theta(i) = \left\{\frac{P_{12}(i)}{2\Delta r}\right\}u(i+1) + \left\{\frac{P_{11}(i)}{r(i)}\right\}u(i) - \left\{\frac{P_{12}(i)}{2\Delta r}\right\}u(i-1) - D(i)\{T(i) - T_0\}, \quad (7b)$$

$$\tau_r(i) = \eta H_0^2 \left\{\frac{u(i+1)}{2\Delta r} - \frac{u(i)}{r(i)} - \frac{u(i-1)}{2\Delta r}\right\}. \quad (7c)$$

The details of finite-difference modeling of governing equation, as well as boundary conditions, are available in [23].

## 4. Modeling of Temperature Fields

### 4.1. Formulation of temperature fields

For an axisymmetric non-uniform FGM disk the transient conduction-convection equation with an internal heat source, $\dot{g}$ is [23,38]:

$$\frac{\partial^2 T}{\partial r^2} + \left\{\frac{1}{r} + \frac{1}{h(r)}\frac{\partial h(r)}{\partial r} + \frac{1}{k(r)}\frac{\partial k(r)}{\partial r}\right\}\frac{\partial T}{\partial r} + \frac{\dot{g}}{k(r)} - \frac{2h_c}{h(r)k(r)}\{T(r) - T_0\} = \left\{\frac{\rho(r)C_p(r)}{k(r)}\right\}\frac{\partial T}{\partial t}. \quad (8)$$

The initial and boundary conditions of the disk are assumed as follows:

$$T(r,t) = T_0 \ \ at\ t = 0, \quad (9a)$$

$$T(a,t) = T_a \ \ at\ t > 0, \quad (9b)$$

$$T(b,t) = T_b \ \ at\ t > 0. \quad (9c)$$

Now, by solving Eq. (8) with associate initial and boundary conditions the transient temperature field of the disk can be obtained.

Eq. (8) can be reduced for steady-state temperature field as follows [23]:

$$\frac{d^2T}{dr^2}+\left\{\frac{1}{r}+\frac{1}{h(r)}\frac{dh(r)}{dr}+\frac{1}{k(r)}\frac{dk(r)}{dr}\right\}\frac{dT}{dr}+\frac{\dot{g}}{k(r)}-\frac{2h_c}{h(r)k(r)}\{T(r)-T_0\}=0. \quad (10)$$

### 4.2. Solution of heat conduction equations

Likewise, displacement and stress fields, FDM is also adopted to obtain the solution of steady-state as well as transient heat conduction equations. Central difference formulae are adopted for position derivative and backward difference formulae are implemented for time derivative. To evaluate the temperature fields, the equal number of nodal points with the equal mesh size are considered like equation (6). So, the size of each mesh is, $\Delta r = (b-a)/(N-1)$. The finite-difference expression of Eq. (8) is [23]:

$$T^j(i)=\left\{1-\frac{2\alpha_T(i)\Delta t}{\Delta r^2}-\frac{2h_c\alpha_T(i)\Delta t}{h(i)k(i)}\right\}T^{j-1}(i)$$
$$+\left[\left[\frac{1}{r(i)}+\frac{1}{h(i)}\left\{\frac{h(i+1)-h(i-1)}{2\Delta r}\right\}+\frac{1}{k(i)}\left\{\frac{k(i+1)-k(i-1)}{2\Delta r}\right\}\right]\left\{\frac{\alpha_T(i)\Delta t}{2\Delta r}\right\}\right.$$
$$\left.+\left\{\frac{\alpha_T(i)\Delta t}{\Delta r^2}\right\}\right]\{T^{j-1}(i+1)-T^{j-1}(i-1)\}+\frac{\dot{g}\alpha_T(i)\Delta t}{k(i)}+\frac{2h_c\alpha_T(i)\Delta tT_0}{h(i)k(i)}. \quad (11)$$

Where, $\alpha_T(i)=\frac{k(i)}{\rho(i)C_p(i)}$. Here, $i$ ($i$ = 1,2,3…$N$) represents the number of nodes and the time steps of the solution are denoted by superscript $j$ ($j$ =1,2,3….). To obtain the transient temperature field Eq. (11) is implemented at the inner nodes ($i$ = 2: $N$-1) of the disk. At initial state, when $t$ = 0 ($j$ = 1) every nodal points ($i$ =1: $N$) are assumed to be at room temperature, $T_0$. From next time steps

($j$=2,3,4,5…..), temperature distribution at inner nodal points ($i$ = 2:$N$-1) of the disk is obtained following Eq. (11) for the fixed inner and outer ends temperature. The critical time steps to obtain the transient temperature field is kept [23,38]

$$\Delta t \leq \frac{1}{\frac{2\alpha_T(i)}{\Delta r^2} + \frac{2h_c\alpha_T(i)}{h(i)k(i)}}. \tag{12}$$

The finite-difference form of Eq. (10) using the central difference formulae is [23]:

$$\left[\frac{1}{\Delta r^2} + \left[\frac{1}{r(i)} + \frac{1}{k(i)}\left\{\frac{k(i+1)-k(i-1)}{2\Delta r}\right\} + \frac{1}{h(i)}\left\{\frac{h(i+1)-h(i-1)}{2\Delta r}\right\}\right]\frac{1}{2\Delta r}\right]T(i+1)$$
$$-\left\{\frac{2}{\Delta r^2} + \frac{2h_c}{k(i)h(i)}\right\}T(i)$$
$$+\left[\frac{1}{\Delta r^2}\right.$$
$$-\left[\frac{1}{r(i)} + \frac{1}{k(i)}\left\{\frac{k(i+1)-k(i-1)}{2\Delta r}\right\} + \frac{1}{h(i)}\left\{\frac{h(i+1)-h(i-1)}{2\Delta r}\right\}\right]\frac{1}{2\Delta r}\right]T(i$$
$$-1) = -\frac{\dot{g}}{k(i)} - \frac{2h_cT_0}{k(i)h(i)}. \tag{13}$$

Again, $i$ ($i$ = 1,2,3…$N$) represents the number of nodes. Applying Eq. (13) at the inner nodes ($i$ = 2: $N$-1) of the disk, the steady-state temperature field with different distributions of material properties and non-uniform thickness profile can be calculated.

## 5. Different Cases of Non-Uniform Thickness Variation

In the equal mass analysis, the mass of different cases of the non-uniform FGM disk is kept as same as the uniform disk. The mass of a uniform disk can be equaled with the mass of a non-uniform FGM disk as [18]:

$$\int_a^b 2\pi r t_0 \rho(r) dr = \int_a^b 2\pi r h(r) \rho(r) dr. \tag{14}$$

In this paper, three different cases of thickness profile variation are considered to study the effect of non-uniform thickness variation on the magneto-thermo-elastic response of a rotating FGM circular disk. In all three cases, the non-uniform FGM disk mass is kept as same as a uniformly thick disk. Three different cases of thickness profile are taken as:

Case-I: Linearly varying thickness profile

$$h(r) = \beta r + \gamma, \tag{15a}$$

Case-II: Rationally varying thickness profile

$$h(r) = \frac{\beta}{r} + \gamma, \tag{15b}$$

Case-III: Exponentially varying thickness profile

$$h(r) = \gamma e^{-\beta r}. \tag{15c}$$

Here, the unknown constants $\beta$ and $\gamma$ can be obtained by the equal mass solution of the uniform and non-uniform FGM disk. Outer end thickness of the rotating non-uniform FGM disk is expressed with respect to the uniform thickness of the disk, $t_0$

$$h(b) = q t_0. \tag{16}$$

Constant, $q$ varies between 0 to 1 ($0<q<1$). In this article, three different values of $q$ are taken as 1/4, 1/2, and 3/4, i.e., when $q$ = 1/4 the outer end thickness of the disk is $h(b) = t_0/4$, and so on for other values of $q$. Now, with the expressions of Eqs. (15) and solving Eq. (14) and (16), constants $\beta$ and $\gamma$ are obtained for every non-uniform thickness variation case.

The details of the computational procedure of determining the magneto-thermo-elastic fields of a rotating FGM disk is illustrated in Figure 2.

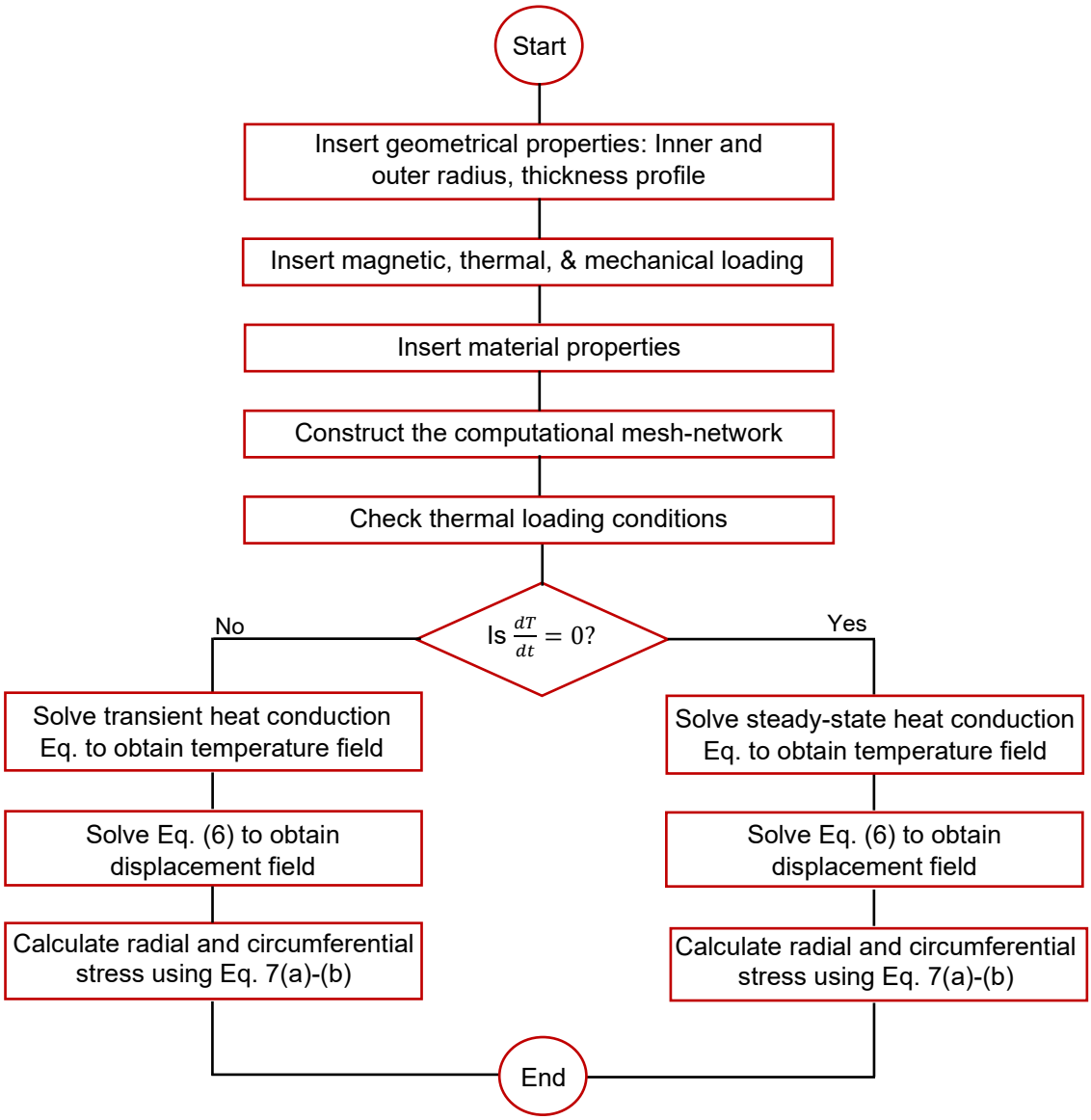


**Figure 2**: Flow-chart determining the magneto-thermo-elastic fields of an FGM disk for both steady-state and transient thermal loading conditions.

## 6. Results and Discussion

In the current work, an $Al/Al_2O_3$ disk was considered to investigate the effect of thickness profiles variation on the magneto-thermo-elastic behavior of a non-uniform FGM rotating disk. The inner and outer ends of the FGM disk are made of Al (material *A*) and $Al_2O_3$ (material *B*), respectively. The mechanical and thermal properties of Al and $Al_2O_3$ are given in Table 1. To analyze the results, the inner radius $a = 0.015$ m and outer radius $b = 0.15$ m is considered. The thickness of the uniform disk is taken as, $t_0 = 10$ mm. Poisson's ratio ($\mu = 0.3$), as well as magnetic permeability, are uniform over the disk. The results are plotted for the magnetic permeability of, $\eta = \eta_0 k_m$, where, $\eta_0 = 4\pi\times10^{-7}$ N/A$^2$ and $k_m = 2.30$. The room temperature is taken as $T_0 = 20$ °C, and the disk is assumed to rotate in the clockwise direction with, $\omega = 100$ rad/s. The disk radius is equally divided into $N = 121$ number of nodes. So, the size of each mesh is, $\Delta r = 0.0015$ m. To verify the present solution, the identical problem is solved in commercially available finite-element software keeping the number of nodes and mesh size equal to the FDM analysis. The convergence and the accuracy of both FDM and FEM solutions have been verified by varying the number of nodes and mesh size, and the well converged results are plotted for the mesh size of 0.0015 m. The excellent agreement between FDM and FEM solutions confirms the validity of the temperature as well as the stress fields of the non-uniform disk.

The variation of all three cases of non-uniform thickness profile with outer end thickness along the normalized radius of the disk is shown in Figure 3. All the non-uniform thickness profiles are calculated following the approach given in section 5. The mass in every case of the non-uniform disk is made equal to the mass of a uniform disk of, $t_0 = 10$ mm. As we see in Figure 3, inner end thickness of the non-uniform FGM disk increases with the decrease in outer end thickness, and

among three different cases of thickness variation inner end thickness becomes maximum for Case-II rationally varying thickness profile [18].

**Table 1**

Properties of Al and $Al_2O_3$ [24].

| Materials | Properties | | | | |
|---|---|---|---|---|---|
| | $E$ (GPa) | $\alpha$ (/°C) | $\rho$ (kg/m$^3$) | $k$ (W/mK) | $C_p$ (J/kgK) |
| Al | 71 | $23.1\times10^{-6}$ | 2700 | 238 | 900 |
| $Al_2O_3$ | 380 | $8\times10^{-6}$ | 960 | 35 | 780 |

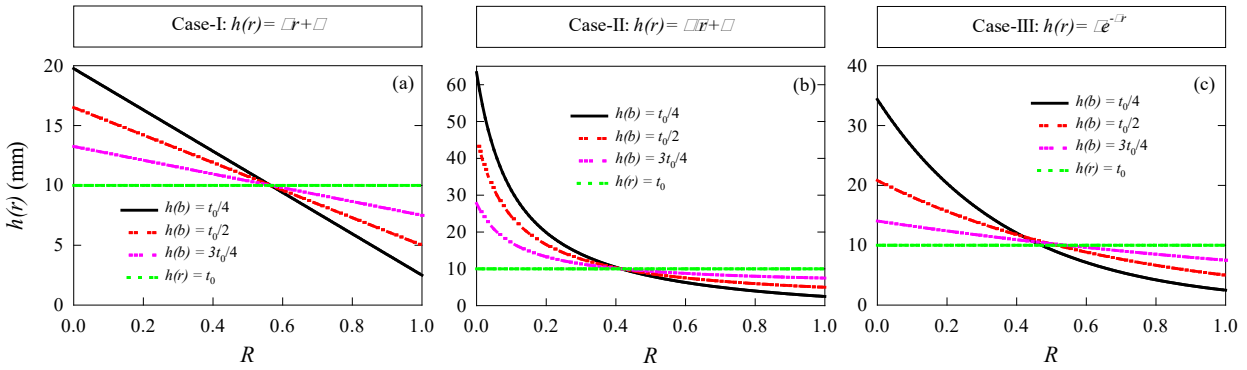


**Figure 3.** Variation of thickness profiles with outer end thickness for (a) Case-I, (b) Case-II, and (c) Case-III thickness variation.

### 6.1. Thermo-elastic field

The stress field of the rotating non-uniform FGM disk ($b/a$ = 10) under the influence of a thermal load is studied for all three cases of non-uniform thickness variation shown in Figure 3. Radial and circumferential stresses are analyzed in absence of the magnetic field ($H_0$ = 0). A steady-state temperature field is considered when the inner end is kept at room temperature, $T_a$ = 20 $^oC$, and the outer end at $T_b$ = 120 $^oC$. An internal heat source of, $\dot{g} = 10^6$ W/m$^3$ is taken and the coefficient of convective heat transfer is kept as, $h_c$ = 25 W/m$^2$K. The temperature distribution profile with outer end thickness for Case-II thickness variation is plotted in Figure 4a. It was found that the decrease in outer end thickness, decreases the distribution of temperature field over the radius, and excellent agreement with FEM results plotted for $h(b) = t_0/4$ verifies the solution of the temperature field.

Figures 4(b)-(d), depcit the distribution of stress components for all three cases of non-uniform thickness profile. Radial stress, $\sigma_r$ plotted in Figures 4(b1)-(d1) is zero at the outer end of the rotating disk which is a good conformity of appropriate modeling of the boundary condition at $R$ = 1. $\sigma_r$ is found to be maximum for uniform disk; with the decrease of outer end thickness, $\sigma_r$ decreases especially in the inner 50% radius of the disk, which shows a good agreement with [14]. For Case-I and Case-III thickness profiles, maximum $\sigma_r$ is occurring at $R$ = 0. But, for Case-II thickness profile, radial stress gets maximum in the intermediate regions between $0<R<0.5$. The distribution of circumferential stress ($\sigma_\theta$) for all three variations of non-uniform thickness profile is illustrated in Figures 4(b2)-(d2). As the outer end thickness decreases, $\sigma_\theta$ increases significantly in the outer 20% disk region of the disk. In Case-I thickness profile maximum $\sigma_\theta$ is found to be higher than maximum $\sigma_r$ when $q$ = 1/4. But, as $q$ increases, maximum $\sigma_r$ dominates over maximum $\sigma_\theta$. For Case-II rationally varying thickness profile, maximum $\sigma_\theta$ is greater than maximum $\sigma_r$ for

any value of $q$. And, for Case-III thickness profile, maximum value of $\sigma_\theta$ is higher than the maximum $\sigma_r$ when $q$ = 1/4 and 1/2. For a uniform disk, the maximum $\sigma_r$ is observed to be greater than maximum $\sigma_\theta$. FEM results plotted for $h(b) = t_0/4$ and uniform disk are also in good agreement with FDM results.

In Table 2, maximum radial stress, $(\sigma_r)_{max}$ and circumferential stress, $(\sigma_\theta)_{max}$ with their location is plotted for all three variations of non-uniform thickness profile and three different values of $h(b)$ with a uniform disk. From Table 2, we can see that $(\sigma_\theta)_{max}$ is significantly higher than $(\sigma_r)_{max}$ in all three cases for an FGM disk of $h(b) = t_0/4$. And, among different cases of thickness variation, $(\sigma_\theta)_{\max}$ is minimum (-59.14 MPa) for Case-I linearly varying thickness profile. Similarly, by varying the thickness profile maximum stress intensity on the disk can also significantly be controlled in case of $h(b) = t_0/4$ and $3t_0/4$. In an apparent comparison of maximum stresses for all three cases of thickness variation, it can be said that optimum stress fields can be found for linear variation of thickness profile. Thus, designing a non-uniform disk with linearly varying thickness will have a higher fatigue life comparing to a disk designed with rational and exponential thickness variations.

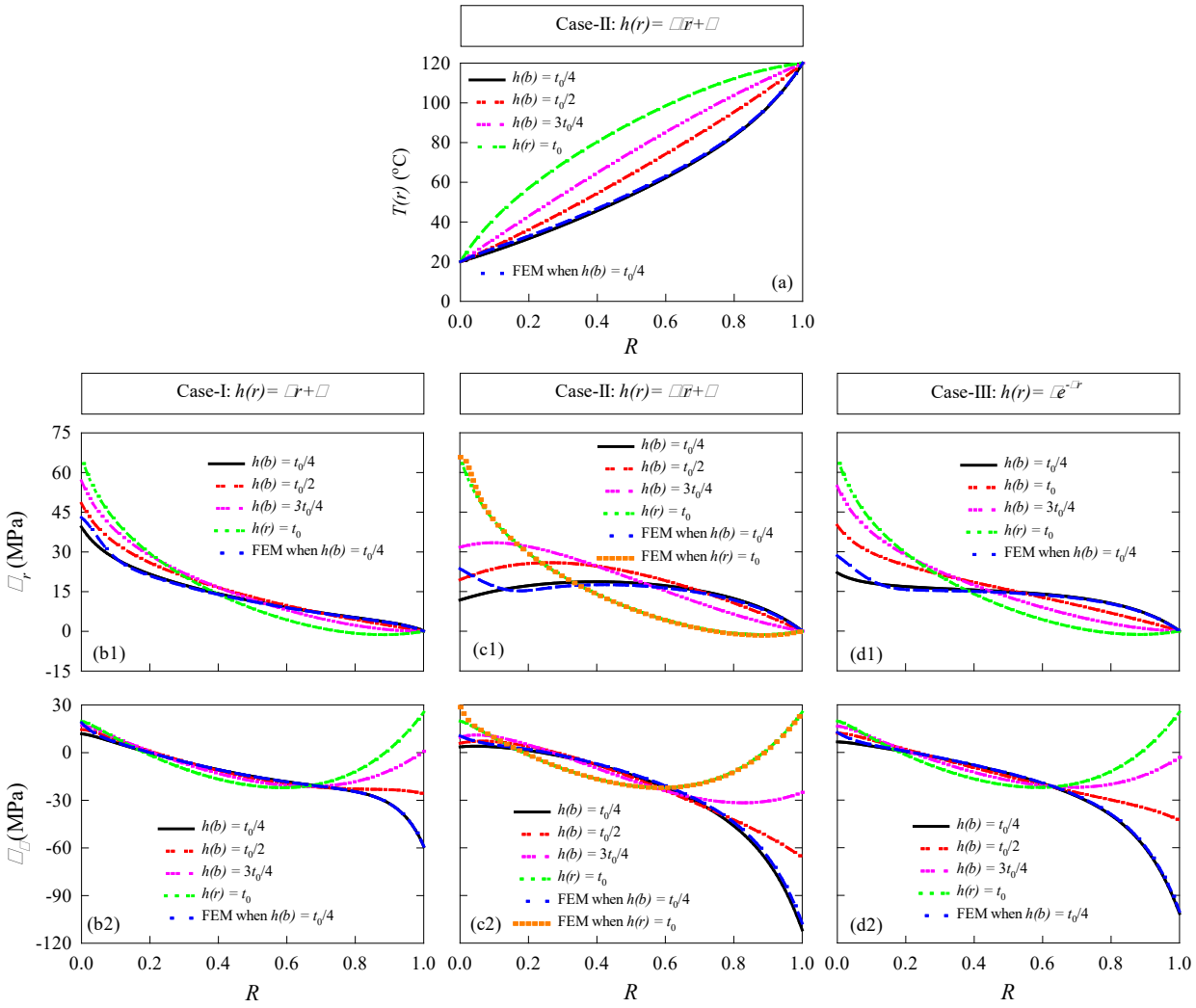


**Figure 4.** Variation of (a) temperature field (for Case-II profile), (b1-d1) radial stress, and (b2-d2) circumferential stress with outer end thickness for all three cases of thickness variation due to thermo-mechanical load ($H_0 = 0$).

**Table 2**

$(\sigma_r)_{max}$ and $(\sigma_\theta)_{max}$ with their location for different cases of thickness profile and outer end thickness.

| Outer end thickness | Maximum radial stress, $(\sigma_r)_{max}$ (MPa) | | | Maximum circumferential stress, $(\sigma_\theta)_{max}$ (MPa) | | |
|---|---|---|---|---|---|---|
| | Case-I | Case-II | Case-III | Case-I | Case-II | Case-III |
| $h(b) = t_0/4$ | 39.5 ($R = 0$) | 18.7 ($R = 0.4$) | 22.1 ($R = 0$) | -59.14 ($R = 1$) | -111.77 ($R = 1$) | -101.5 ($R = 0.075$) |
| $h(b) = t_0/2$ | 48.37 ($R = 0.4$) | 25.87 ($R = 0.258$) | 40.002 ($R = 0$) | -26.1 ($R = 1$) | -66.16 ($R = 1$) | -42.93 ($R = 0.367$) |
| $h(b) = 3t_0/4$ | 56.92 ($R = 0$) | 33.42 ($R = 0.092$) | 54.75 ($R = 0$) | -21.33 ($R = 0.67$) | -31.7 ($R = 0.825$) | -22.1 ($R = 0.692$) |
| $h(r) = t_0$ | 65.68 ($R = 0$) | | | 25.44 ($R = 1$) | | |

### 6.2. Magneto-thermo-elastic fields

Now, the stress fields for all three non-uniform cases of thickness variation are analyzed considering the presence of a steady-state magnetic field for the same FGM disk of $b/a = 10$ rotating in a magnetic field of, $H_0 = 2.23\times10^8$ A/m. The thermal loading conditions are kept as same as mentioned in section 6.1.

The distribution of radial stress, $\sigma_r$ with outer end thickness is plotted in Figures 5(a1)-(c1). The presence of the magnetic field increases $\sigma_r$ over the disk radius in all three cases of thickness variation (see Figs. 4 and 5). For Case-II thickness profile as shown in Figure 5(b1), magnetic field shifts the position of maximum $\sigma_r$ from the intermediate region of $0<R<0.5$ to $R = 0$ in all three values of $q$. The distribution of circumferential stress, $\sigma_\theta$ is plotted in Figures 5(a2)-(c2), and it is observed that in presence of the magnetic field, the magnitude of compressive $\sigma_\theta$ decreases, especially at the outer region of the FGM disk.

For Case-I thickness profile at $H_0 = 0$ (Figures 4b), maximum $\sigma_\theta$ was higher than maximum $\sigma_r$ when $q$ = 1/4. But, when magnetic field is present, as we see in Figures 5a, for any value of $q$ maximum $\sigma_r$ is found to be higher than maximum $\sigma_\theta$. For Case-II thickness profile when $H_0 = 0$ (Figures 4c) maximum value of $\sigma_\theta$ was always higher than maximum $\sigma_r$, but in the presence of the magnetic field, maximum $\sigma_r$ dominates over maximum $\sigma_\theta$ except for $q$ =1/4. For Case-III thickness profile at $H_0 = 0$ (Figures 4d) maximum intensity of $\sigma_\theta$ was higher than maximum $\sigma_r$ when $q$ = 1/4 and 1/2. In presence of the magnetic field, magnitude of radial stress is almost as same as circumferential stress for $q$ = 1/4, but when $q$ = 1/2 and 3/4 radial stress becomes higher than circumferential stress. So, from the analysis above, it can be stated that along with effecting magnitude, magnetic field can also change the nature and location of the maximum stress of the disk.

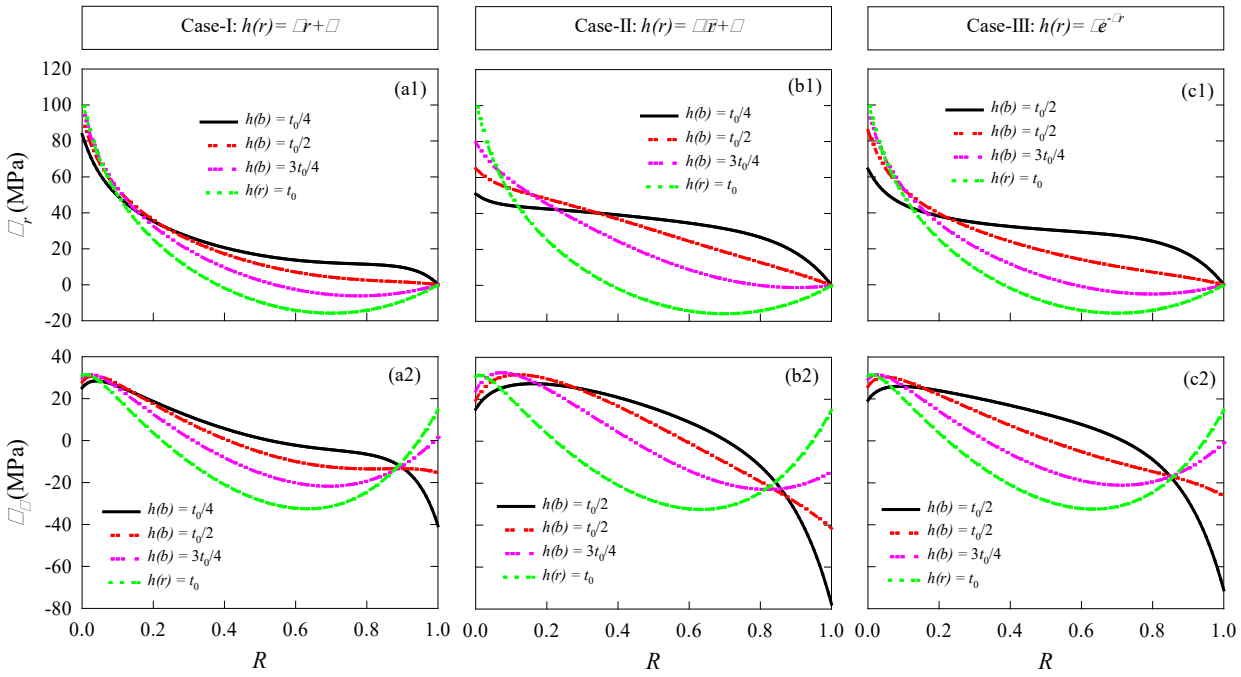


**Figure 5.** Variation of radial stress and circumferential stress with outer end thickness for (a1-a2) Case-I, (b1-b2) Case-II, and (c1-c2) Case-III thickness variation due to magneto-thermo-mechanical load ($H_0 = 2.23\times10^8$ A/m).

### 6.3. Effect of magnetic field

The effect of magnetic field on the components of stress is analyzed here for all three variations (Cases-I-III) of non-uniform thickness profile for an FGM disk of $h(b) = t_0/4$ and five different intensities of, $H_0$. The distribution of radial stress, $\sigma_r$ with $H_0$ is plotted in Figures 6(a1)-(c1). As $H_0$ increases, $\sigma_r$ increases across the radius, and the increment rate is very significant near $R = 0$. For Case-I and III thickness profiles, $\sigma_r$ stays maximum at $R = 0$ for any value of $H_0$, but for Case-II thickness profile magnetic field changes the position of maximum $\sigma_r$ from intermediate region to $R = 0$ when $H_0 \geq 10^8$ A/m (see Figure 6(b1)). With the increase in $H_0$, compressive zone on circumferential stress, $\sigma_\theta$ (Figures 6(a2)-(c2)) decreases and at the high intensity of magnetic field vector ($H_0 = 2.23\times10^9$ A/m) $\sigma_\theta$ gets tensile almost over the disk for all three cases of thickness variation.

Now, in Figure 7, $(\sigma_r)_{max}$ and $(\sigma_\theta)_{max}$ are plotted to analyze the variation of maximum stress with magnetic field and thickness profiles for a disk of $h(b) = t_0/4$. As we see in Figure 7, for Case-II thickness profile, when $H_0 = 0$ maximum value of $\sigma_r$ and $\sigma_\theta$ is 18.69 MPa and -111.77 MPa, respectively. But, when $H_0 = 2.23\times10^8$ A/m $(\sigma_r)_{max}$ becomes 50.88 MPa and $(\sigma_\theta)_{max}$ is -77.6 MPa. Similar phenomena occur for Case-III rationally varying thickness profile as shown in Figure 7. So, with an optimum intensity of $H_0$, the high-stress intensity in case of Case-II and III thickness profiles (when $H_0 = 0$) can be decreased drastically which will significantly increase the fatigue life cycle of the rotating non-uniform disk.

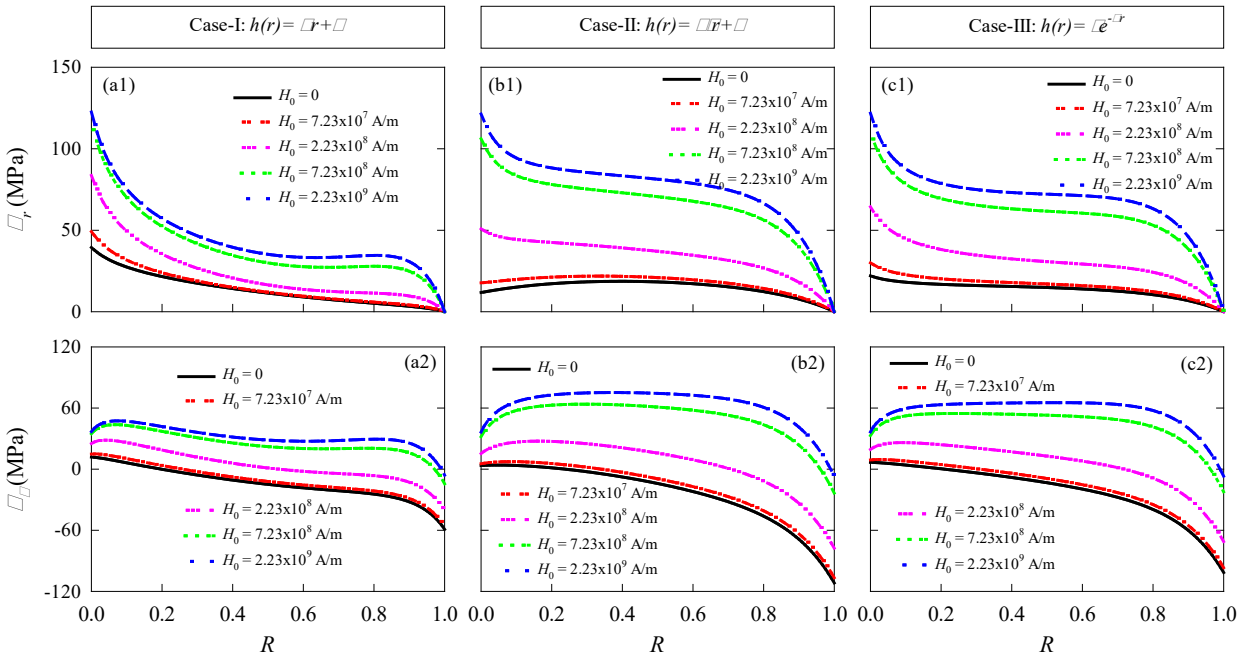


**Figure 6.** Variation of radial stress and circumferential stress with $H_0$ for (a1-a2) Case-I, (b1-b2) Case-II, and (c1-c2) Case-III thickness variation for a disk of, $h(b) = t_0/4$.

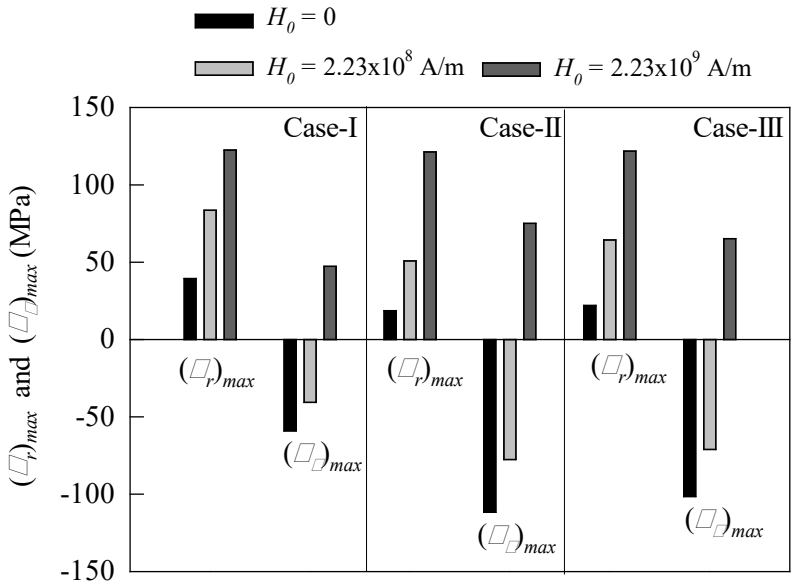


**Figure 7.** Maximum radial stress and circumferential stress for all three non-uniform thickness profiles and three different intensities of $H_0$ for a disk with $h(b) = t_0/4$.

### 6.4. Transient stress analysis

In this section, variation of stress fields with thickness profiles is analyzed for the transient condition of temperature field. Initially, the transient stress fields are analyzed at different time sections for Case-II rationally varying thickness profile for an FGM disk of $h(b) = t_0/4$ and $b/a = 10$, rotating at $\omega = 100$ rad/s. Later, the variation of stress fields with outer end thickness and different cases of non-uniformly varying thickness at different positions of the rotating disk is also analyzed in the time period of $1\text{s} \leq t \leq 60\text{s}$.

In Figure 8, distribution of stress fields with time and $H_0$ is plotted at different time sections of the transient temperature field. The associated temperature field is taken for $T_a = 20$ ºC, $T_b = 120$ ºC, $\dot{q} = 10^6$ W/m$^3$, and $h_c = 25$ W/m$^2$K at six different time section from $t = 2$s to $\infty$. The associate transient temperature field is similar to the one of Figure 8(a) in [23]. The distribution of radial stress, $\sigma_r$ with time is plotted in Figures 8(a1)-(b1) for two different magnitudes of $H_0$. At initial state, when magnetic field is absent ($H_0 = 0$), the high intensity of $\sigma_r$ is observed at $R = 0.85$ zones, but as time progresses, the intensity of maximum $\sigma_r$ shifts towards the inner region of the rotating disk and at steady-state temperature field $\sigma_r$ gets maximum at $R = 0.4$. In presence of the magnetic field ($H_0 = 2.23\times10^8$ A/m), radial stress gets maximum near $R = 0.8$ regions at the initial state of time, but the maximum value of $\sigma_r$ decreases with time, and at steady-state it is found to be maximum at the inner end. Distribution of $\sigma_\theta$ with time and $H_0$ is plotted in Figures 8(a2)-(b2). $\sigma_\theta$ is found to be maximum at the outer end and the maximum value of $\sigma_\theta$ is greater than maximum $\sigma_r$. The presence of magnetic field reduces the compressive nature of $\sigma_\theta$ in Figure 8(b2). At any time section for both $H_0 = 0$ and $2.23\times10^8$ A/m, maximum $\sigma_\theta$ stays higher than maximum $\sigma_r$. Excellent agreement with FEM results in Figures 8(a1)-(a2) at $t = 5$s confirms the proper modeling of transient stress fields.

Variation of $\sigma_r$ and $\sigma_\theta$ with time and outer end thickness is plotted in Figure 9 for Case-II thickness profile at different positions of the disk ($R$ = 0, 0.8, and 1) for the magnetic field vector of $H_0 = 2.23\times10^8$ A/m. As shown in Figure 9, $\sigma_r$ at $R$ = 0 increases and $R$ = 0.8 decreases with the progress of time showing a good agreement with Figure 8(b1). With the increase in outer end thickness, distribution of $\sigma_r$ increases at $R$ = 0 and decreases at $R$ = 0.8 when $t$>10s. $\sigma_\theta$ (Figure 9(b1)) at $R$ = 0.8 is tensile at the initial state and with the progress of time, it becomes compressive. As the outer end thickness increases, the positive nature of $\sigma_\theta$ at $R$ = 0.8 increases significantly at the initial state. The compressive nature of circumferential stress at $R$ = 1 (Figure 9(b2)) decreases with time and outer end thickness. As time progresses, with the increase in outer end thickness maximum $\sigma_r$ (Figure 9(a1)) exceeds the maximum $\sigma_\theta$ (Figure 9(b2)).

Variation of $\sigma_r$ and $\sigma_\theta$ with time and three different cases of thickness profile for a disk of $h(b) = t_0/4$ is plotted in Figure 10 at $R$ = 0 and 1, respectively. As we see in Figure 10a, the distribution of $\sigma_r$ at $R$ = 0 stays maximum for Case-I linearly varying thickness profile and minimum for Case-II rational variation of thickness profile over the time domain. With the progress of time, $\sigma_\theta$ at $R$ = 1 shows some variation for Case-I thickness profile, but no significant variation of with Case-II and III thickness profiles is observed over the time domain as shown in Figure 10b.

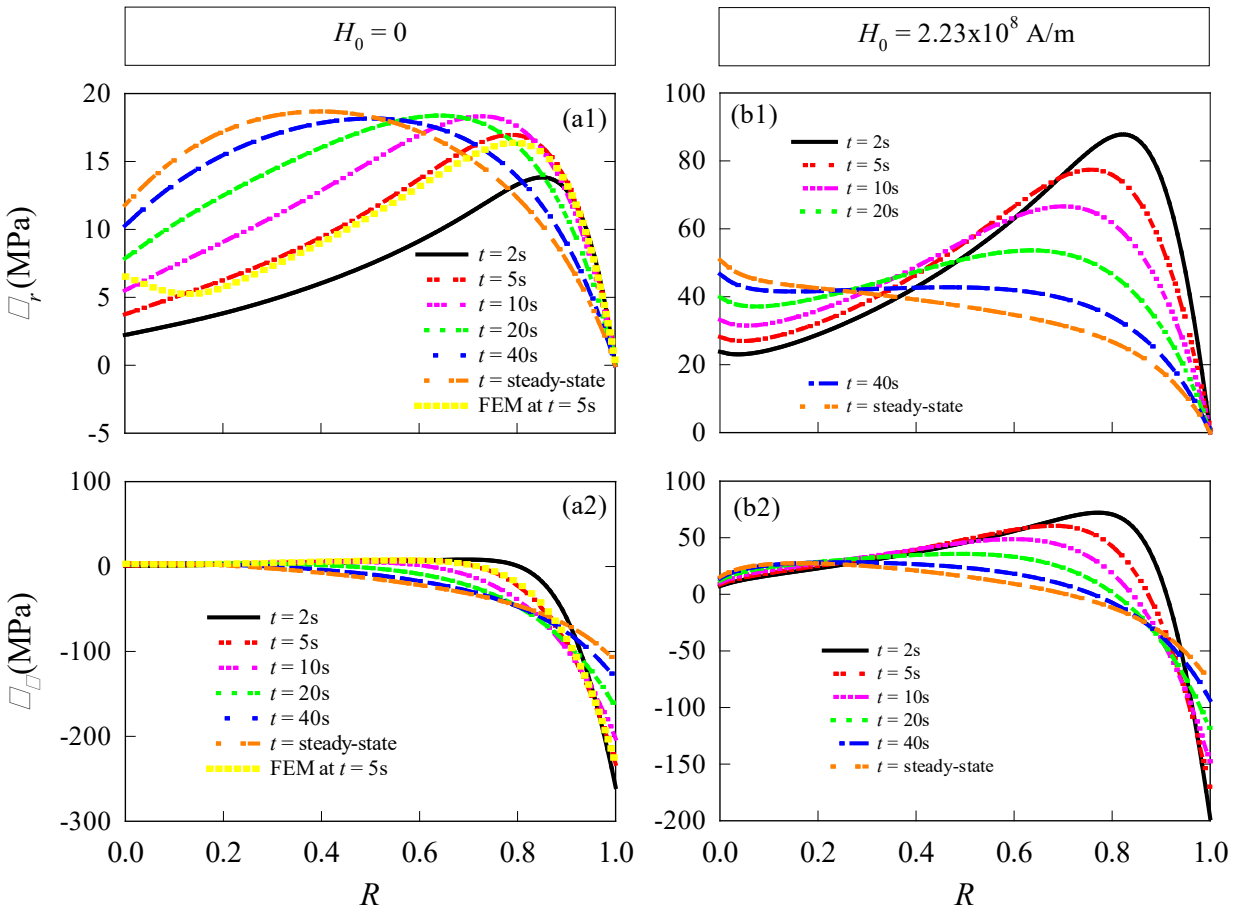


**Figure 8.** Variation of radial stress and circumferential stress fields with time for Case-II (*h(b)* = $t_0/4$) thickness profile when: (a1-a2) $H_0 = 0$, and (b1-b2) $H_0 = 2.23\times10^8$ A/m.

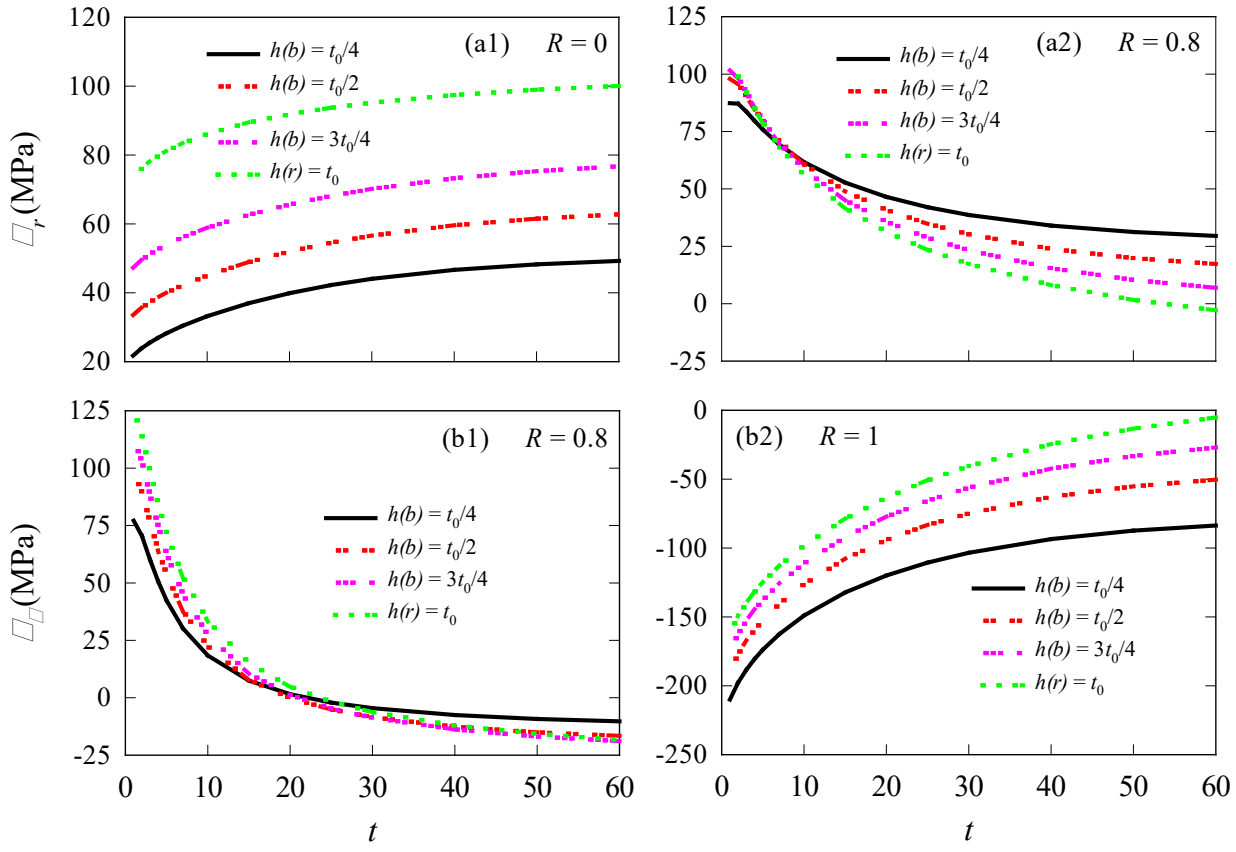


**Figure 9.** Variation of (a1-a2) radial stress at $R = 0$ and 0.8, and (b1-b2) circumferential stress at $R = 0.8$ and 1 with time and outer end thickness for Case-II rationally varying thickness profile in a magnetic field of $H_0 = 2.23\times10^8$ A/m.

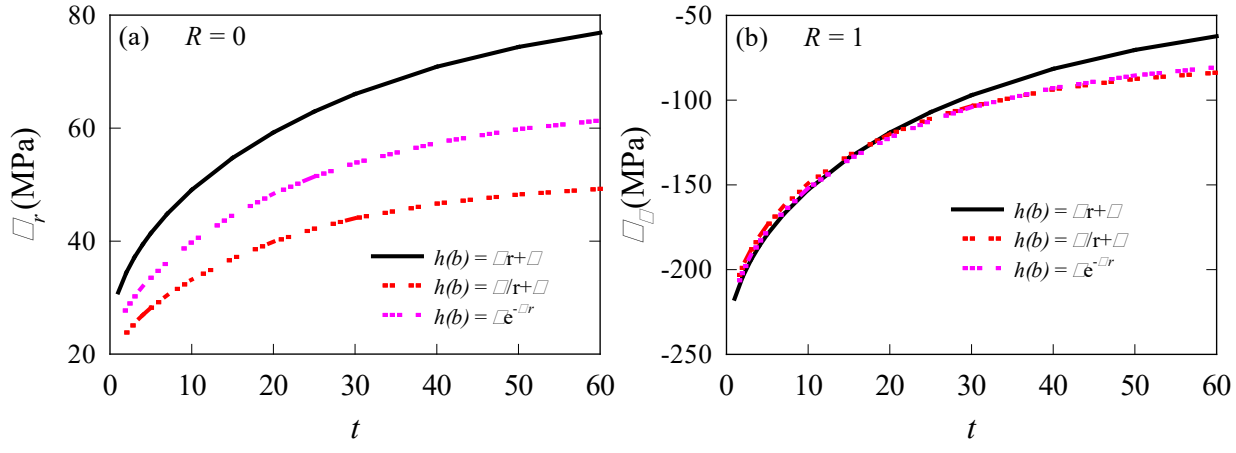


**Figure 10.** Variaton of (a) $\sigma_r$ at $R = 0$, and (b) $\sigma_\theta$ at $R = 1$ with time and different cases of thickness profile for $h(b) = t_0/4$ and $H_0 = 2.23\times10^8$ A/m.

### 6.5. Effect of material properties

In previous sections, magneto-thermo-elastic fields were analyzed for exponentially varying material properties. The effect of material properties on the magneto-thermo-elastic fields is investigated here for Case-II rationally varying thickness profile for an FGM disk of $h(b) = t_0/4$ and $b/a = 10$, rotating with $\omega = 100$ rad/s. To investigate the effect, material properties are considered to vary following the power-law of distribution across the radius of the disk according to Eq. (2). Four different values of the power-law index, $n$ are considered to analyze the effect of material properties. Steady-state as well as transient conditions of temperature fields are considered when $T_a = 20$ ºC, $T_b = 120$ ºC, $\dot{q} = 10^6$ W/m$^3$, and $h_c = 25$ W/m$^2$K.

In Figure 11, variation of $\sigma_r$ and $\sigma_\theta$ is plotted with $n$ and two different magnitudes of magnetic field vector, $H_0 = 0$, and $2.23\times10^8$ A/m. When the magnetic field is absent ($H_0 = 0$), $\sigma_r$ is tensile over the disk radius, and the distribution of $\sigma_r$ decreases with the increase of $n$. Like E-FGM here again when $H_0 = 0$, maximum $\sigma_r$ is found in the intermediate regions of $0.2<R<0.3$. $\sigma_\theta$ decreases with the increase of $n$ and for any value of $n$, $\sigma_\theta$ is higher than $\sigma_r$ when $H_0 = 0$ (see Figures 11a). When the magnetic field is present with $H_0 = 2.23\times10^8$ A/m, radial stress in Figure 11(b1) is tensile over the disk for the smaller value of $n$, and as $n$ increases, $\sigma_r$ tends to be compressive near the outer end. Magnetic field changes the location of maximum $\sigma_r$ and for any values of $n$ when magnetic field is present, maximum $\sigma_r$ is found at $R = 0$. When magnetic field is present, the compressive intensity of $\sigma_\theta$ near the outer region decreases as we see in Figures 11(b1)-(b2). $\sigma_\theta$ is higher than $\sigma_r$ when $n = 1$, but for higher values of $n$, $\sigma_r$ dominates over $\sigma_\theta$.

Variation of $\sigma_r$ and $\sigma_\theta$ with time and gradient index, $n$ is illustrated in Figure 12 for the disk of $h(b) = t_0/4$ of Case-II rationally varying thickness profile. As shown in Figures 12(a)-(b), like E-FGM disk, stress intensity gets high at the beginning of time for a P-FGM disk of $n = 4$, and as

time progresses, the high-stress intensity minimizes. At initial state, maximum $\sigma_\theta$ is higher than maximum $\sigma_r$. But, as time progresses, the intensity of $\sigma_r$ increases near the inner end of the non-uniform disk, and $\sigma_\theta$ intensity near $R$ = 1 decreases keeping similarity with Figure 8 of E-FGM disk.

In Figures 12(b1)-(b2), variation of $\sigma_r$ and $\sigma_\theta$ is plotted with time and gradient index, $n$ at $R$ = 0 and 1, respectively. The non-linear distribution of $\sigma_r$ at $R$ = 0 increases with the increase of time and $n$. The compressive nature of $\sigma_\theta$ at $R$ =1 decreases with the increase of time and gradient-index $n$ as we see in Figure 12(b2).

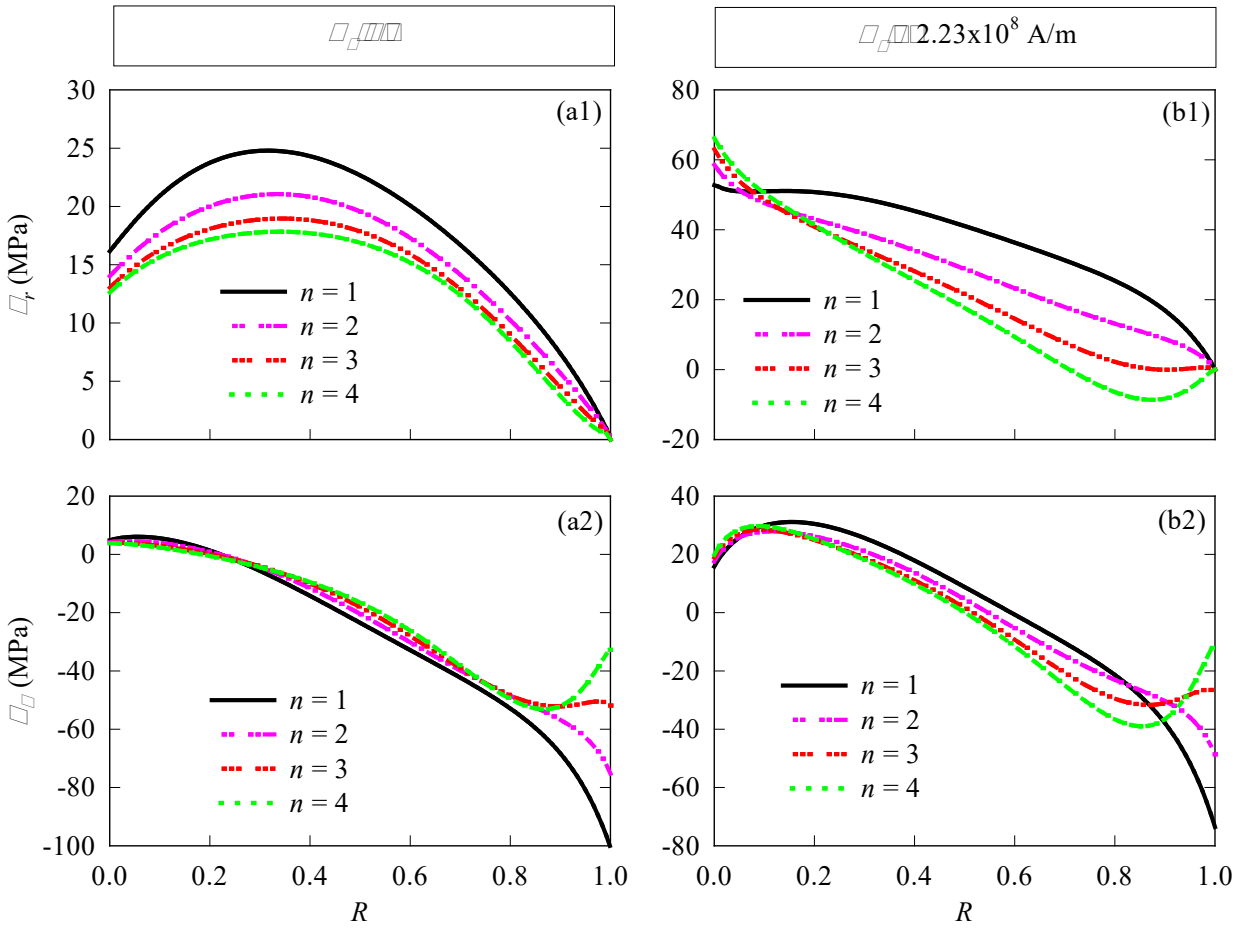


**Figure 11.** Variation of radial stress and circumferential stress field with gradient index, $n$ for Case-II ($h(b) = t_0/4$) thickness profile when: (a1-a2) $H_0$ = 0, and (b1-b2) $H_0 = 2.23\times10^8$ A/m

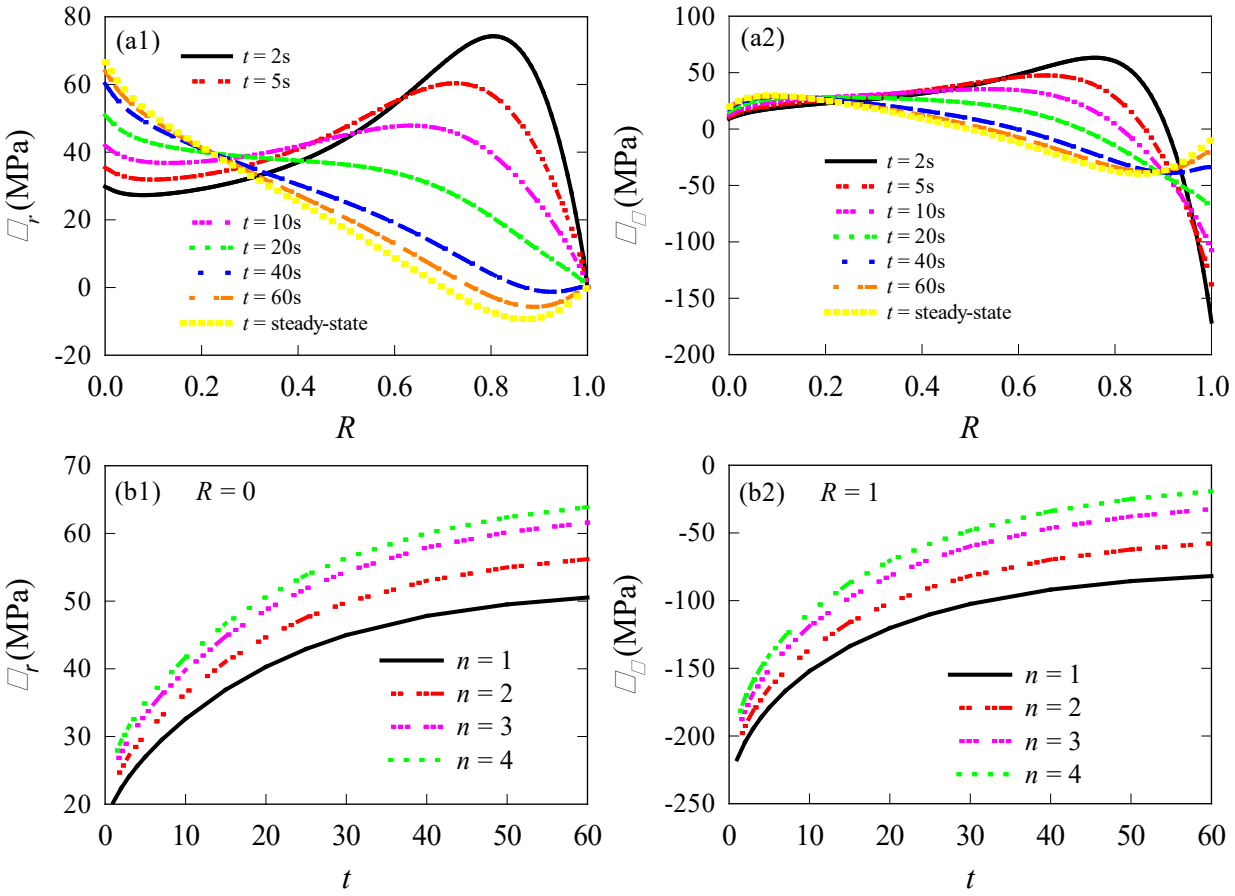


**Figure 12.** Variation of radial stress and circumferential stress field (a1-a2) with time for $n = 4$, and (b1-b2) with time and gradient index, $n$ for Case-II: $h(b) = t_0/4$ P-FGM disk ($H_0 = 2.23\times10^8$ A/m).

## 7. Comparison of the Results with Analytical Solution

The comparison of the FDM solution with FEM solution in previous sections verified the temperature as well as stress field distributions of the FGM disk. In this section, a comparison with an analytical solution is made to check the convergence and consistency of the numerical solution. It is worth mentioning that any authentic and reliable analytical solution of the stress field of a rotating non-uniform FGM disk in magneto-thermal environment can hardly be found in the literature. So, we compare the FDM solution with the corresponding analytical solution of a uniform isotropic disk. In this approach, a comparison is made with the analytical results found in Bayat et al. [16] for a uniform isotropic rotating disk in magneto-thermal environment. Keeping the notations as same as our paper the governing ordinary differential equation [Eq. (10)] of Bayat et al. [16] for the uniform isotropic rotating disk under a uniform temperature field placed in a magnetic field can be written as:

$$\frac{d^2u}{dr^2}+\frac{1}{r}\frac{du}{dr}-\frac{1}{r^2}u=-\left\{\frac{(1-\mu^2)}{E+(1-\mu^2)\eta H_0^2}\right\}\rho r\omega^2. \tag{17}$$

Now, solving Eq. (17) the analytical solution of radial displacement is

$$u=\ C_1 r+\frac{C_2}{r}-\left\{\frac{(1-\mu^2)\rho\omega^2}{8(E+(1-\mu^2)\eta H_0^2)}\right\}r^3. \tag{18}$$

Here, the constants $C_1$ and $C_2$ are obtained from the boundary conditions given in section 2. To apply the finite-difference model used in this paper for the uniform isotropic disk, the parameter $n_m = 0$ into Eq. (1) and $h(r) = t_0$ are considered.

In Table 3, the comparison between FDM with analytical results is made for an Aluminum disk of $b/a = 10$ and $t_0 = 10$ mm. The disk is divided into $N = 121$ number of nodes to obtain the FDM solution. A steady-state uniform temperature field of $T(r) = 120$ ºC and angular speed $\omega = 100$

rad/s is considered keeping the magnetic field vector, $H_0 = 2.23\times10^8$ A/m. To compare the results, radial displacement and radial stress at different positions on the disk are plotted in Table 3 for both FDM and analytical results. From Table 3, it is clear that FDM results for both radial displacement and radial stress at different positions on the disk completely match with analytical results confirming that our finite-difference analysis is based on sound philosophy and reliable. Furthermore, the excellent agreement of FDM solution with analytical solution at different positions of the disk confirms the convergence as well as consistency of our numerical solution over the disk radius. Thus, it can be concluded that this FDM analysis can be used to solve FGM circular disk problems along with other available approaches.

**Table 3**

Comparison of the analytical and FDM solutions obtained for the isotropic disk.

| Solutions | Radial displacement, $u$ (mm) | | | Radial stress, $\sigma_r$ (MPa) | | |
|---|---|---|---|---|---|---|
| | $R = 0.25$ | $R = 0.5$ | $R = 1$ | $R = 0$ | $R = 0.25$ | $R = 0.5$ |
| Analytical results | 0.101441 | 0.183348 | 0.341274 | 0.124364 | 0.010708 | 0.002956 |
| FDM | 0.101434 | 0.183343 | 0.341271 | 0.122490 | 0.010721 | 0.002959 |

## 8. Summary

The stress field of an FGM circular disk is analyzed in the magneto-thermal environment for three different cases of non-uniform thickness variation. Linear, rational, and exponential functions of disk radius are considered to vary the thickness profile while the mass of the disk were kept equal in all uniform and non-uniform cases of thickness variations. The finite-difference method is adopted to solve the associated differential equations. The effect of the magnetic field, transient stress fields, and effect of material properties are analyzed in the perspective of non-uniform thickness variations. Few key findings of this work are summarized as follows:

1. When magnetic field is absent, the decrease in outer end thickness significantly increases $\sigma_\theta$ at the outer end of the rotating FGM disk, especially in case of rational and exponential variation of the thickness profiles.
2. Maximum $\sigma_\theta$ (when $H_0 = 0$) at the outer end of the disk is found to be higher than the maximum $\sigma_r$ in all three cases of thickness variation for a disk of $h(b) = t_0/4$. Increase in outer end thickness and the presence of magnetic field change both the location and nature of maximum stress.
3. In absence of magnetic field, for a disk with thin outer end (e.g., $h(b) = t_0/4$), minimum stress fields can be found for linear variation of thickness profile. And, high intensity of $\sigma_\theta$ with rationally and exponentially varying thickness profiles can significantly be reduced with an optimum magnetic field.
4. Our analysis showed that by properly selecting the non-uniform thickness profile and with optimum intensity of $H_0$, the maximum stress of the disk can significantly be controlled, which will remarkably increase the disk fatigue life cycle.

5. Transient analysis of stresses showed the distribution of stress fields with time and outer end thickness for different cases of non-uniform thickness profile.
6. For P-FGM disk when magnetic field is absent, $\sigma_\theta$ is higher than $\sigma_r$ for every value of $n$, and in presence of the magnetic field, $\sigma_r$ gets over $\sigma_\theta$ for $n \geq 2$.

Finally, we anticipate that this study will help to design and analysis of uniform/non-uniform FGM disks in various engineering applications under thermal and magneto-thermal environments.

**Acknowledgment:**

The authors would like to thank Department of Mechanical Engineering, Bangladesh University of Engineering and Technology (BUET) for the support and facilities provided in this work.

**Conflict of Interest:**

The author(s) declare there is no conflict of interest in this article.

**Nomenclature**

| | |
|---|---|
| $\sigma_\theta$ | circumferential stress |
| $E(r)$ | modulus of elasticity |
| $\alpha(r)$ | thermal expansion coefficient |
| $\rho(r)$ | mass density |
| $h(r)$ | thickness profile |
| $k(r)$ | thermal conductivity |
| $C_p(r)$ | specific heat |
| $h_c$ | convection heat transfer coefficient |
| $t$ | time |
| $\mu$ | Poisson's ratio |
| $\eta$ | magnetic permeability |
| $\eta_0$ | magnetic permeability of space |
| $k_m$ | relative permeability |
| $H_0$ | magnetic field vector |
| $T(r)$ | temperature distribution |
| $T_0$ | room temperature |
| $\Delta T = T(r) - T_0$ | temperature difference |
| $R = (r-a)/(b-a)$ | non-dimensional radius |

## References


[1] A.N. Eraslan, T. Akis, On the plane strain and plane stress solutions of functionally graded rotating solid shaft and solid disk problems, Acta Mechanica. 181 (2006) 43–63. https://doi.org/10.1007/s00707-005-0276-5.

[2] W. Tebboune, M. Merdjah, K.H. Benrahou, A. Tounsi, Thermoelastic buckling response of thick functionally graded plates, J Appl Mech Tech Phy. 55 (2014) 857–869. https://doi.org/10.1134/S0021894414050150.

[3] M. Amirpour, R. Das, E.I. Saavedra Flores, Bending analysis of thin functionally graded plate under in-plane stiffness variations, Applied Mathematical Modelling. 44 (2017) 481–496. https://doi.org/10.1016/j.apm.2017.02.009.

[4] P. Malik, R. Kadoli, Thermo-elastic response of SUS316-Al 2 O 3 functionally graded beams under various heat loads, International Journal of Mechanical Sciences. 128–129 (2017) 206–223. https://doi.org/10.1016/j.ijmecsci.2017.04.014.

[5] M.D. Demirbas, Thermal stress analysis of functionally graded plates with temperature-dependent material properties using theory of elasticity, Composites Part B: Engineering. 131 (2017) 100–124. https://doi.org/10.1016/j.compositesb.2017.08.005.

[6] M.D. Demirbas, M.K. Apalak, Thermal stress analysis of one- and two-dimensional functionally graded plates subjected to in-plane heat fluxes, Proceedings of the IMechE. 233 (2019) 546–562. https://doi.org/10.1177/1464420716675507.

[7] H.-L. Dai, Y.-N. Rao, H.-J. Jiang, An analytical method for magnetothermoelastic analysis of functionally graded hollow cylinders, Applied Mathematics and Computation. 218 (2011) 1467–1477. https://doi.org/10.1016/j.amc.2011.06.030.

[8] A. Hajisadeghian, A. Masoumi, A. Parvizi, Investigating the magnetic field effects on thermomechanical stress behavior of thick-walled cylinder with inner FGM layer, Journal of Thermal Stresses. 41 (2018) 286–301. https://doi.org/10.1080/01495739.2017.1399307.

[9] H.-L. Dai, T. Dai, H.-Y. Zheng, Stresses distributions in a rotating functionally graded piezoelectric hollow cylinder, Meccanica. 47 (2012) 423–436. https://doi.org/10.1007/s11012-011-9447-8.

[10] P. Akbari, A. Asanjarani, Semi-analytical mechanical and thermal buckling analyses of 2D-FGM circular plates based on the FSDT, Mechanics of Advanced Materials and Structures. 26 (2019) 753–764. https://doi.org/10.1080/15376494.2017.1410913.

[11] A.M. Zenkour, Analytical solutions for rotating exponentially-graded annular disks with various boundary conditions, Int. J. Str. Stab. Dyn. 05 (2005) 557–577. https://doi.org/10.1142/S0219455405001726.

[12] M. Bayat, M. Saleem, B.B. Sahari, A.M.S. Hamouda, E. Mahdi, Analysis of functionally graded rotating disks with variable thickness, Mechanics Research Communications. 35 (2008) 283–309. https://doi.org/10.1016/j.mechrescom.2008.02.007.

[13] A.M. Zenkour, Steady-state thermoelastic analysis of a functionally graded rotating annular disk, Int. J. Str. Stab. Dyn. 06 (2006) 559–574. https://doi.org/10.1142/S0219455406002064.

[14] T. Dai, H.-L. Dai, Thermo-elastic analysis of a functionally graded rotating hollow circular disk with variable thickness and angular speed, Applied Mathematical Modelling. 40 (2016) 7689–7707. https://doi.org/10.1016/j.apm.2016.03.025.

[15] M. Bayat, B.B. Sahari, M. Saleem, A.M.S. Hamouda, J.N. Reddy, Thermo elastic analysis of functionally graded rotating disks with temperature-dependent material properties: uniform

and variable thickness, Int J Mech Mater Des. 5 (2009) 263–279. https://doi.org/10.1007/s10999-009-9100-z.

[16] M. Bayat, M. Rahimi, M. Saleem, A.H. Mohazzab, I. Wudtke, H. Talebi, One-dimensional analysis for magneto-thermo-mechanical response in a functionally graded annular variable-thickness rotating disk, Applied Mathematical Modelling. 38 (2014) 4625–4639. https://doi.org/10.1016/j.apm.2014.03.008.

[17] A.M. Zenkour, On the magneto-thermo-elastic responses of FG annular sandwich disks, International Journal of Engineering Science. 75 (2014) 54–66. https://doi.org/10.1016/j.ijengsci.2013.11.001.

[18] Y. Zheng, H. Bahaloo, D. Mousanezhad, E. Mahdi, A. Vaziri, H. Nayeb-Hashemi, Stress analysis in functionally graded rotating disks with non-uniform thickness and variable angular velocity, International Journal of Mechanical Sciences. 119 (2016) 283–293. https://doi.org/10.1016/j.ijmecsci.2016.10.018.

[19] Y. Zheng, H. Bahaloo, D. Mousanezhad, A. Vaziri, H. Nayeb-Hashemi, Displacement and Stress Fields in a Functionally Graded Fiber-Reinforced Rotating Disk With Nonuniform Thickness and Variable Angular Velocity, Journal of Engineering Materials and Technology. 139 (2017). https://doi.org/10.1115/1.4036242.

[20] A.M. Eldeeb, Y.M. Shabana, A. Elsawaf, Influences of angular deceleration on the thermoelastoplastic behaviors of nonuniform thickness multilayer FGM discs, Composite Structures. 258 (2021) 113092. https://doi.org/10.1016/j.compstruct.2020.113092.

[21] H.-L. Dai, Z.-Q. Zheng, T. Dai, Investigation on a rotating FGPM circular disk under a coupled hygrothermal field, Applied Mathematical Modelling. 46 (2017) 28–47. https://doi.org/10.1016/j.apm.2017.01.062.

[22] M. Kadkhodayan, M.E. Golmakani, Non-linear bending analysis of shear deformable functionally graded rotating disk, International Journal of Non-Linear Mechanics. 58 (2014) 41–56. https://doi.org/10.1016/j.ijnonlinmec.2013.08.007.

[23] P.R. Sarkar, A.S. Rahman, Effect of magnetic field on the thermo-elastic response of a rotating FGM Circular disk with non-uniform thickness, The Journal of Strain Analysis for Engineering Design. (2021) 03093247211005215. https://doi.org/10.1177/03093247211005215.

[24] A.M. Afsar, J. Go, Finite element analysis of thermoelastic field in a rotating FGM circular disk, Applied Mathematical Modelling. 34 (2010) 3309–3320. https://doi.org/10.1016/j.apm.2010.02.022.

[25] S.-Y. Leu, L.-C. Chien, Thermoelastic Analysis of Functionally Graded Rotating Disks with Variable Thickness Involving Non-Uniform Heat Source, Journal of Thermal Stresses. 38 (2015) 415–426. https://doi.org/10.1080/01495739.2015.1015892.

[26] A. Shaterzadeh, H. Behzad, M. Shariyat, Stability Analysis of Composite Perforated Annular Sector Plates Under Thermomechanical Loading by Finite Element Method, Int. J. Str. Stab. Dyn. 18 (2018) 1850100. https://doi.org/10.1142/S0219455418501006.

[27] A. Hassani, M.H. Hojjati, E. Mahdavi, R.A. Alashti, G. Farrahi, Thermo-mechanical analysis of rotating disks with non-uniform thickness and material properties, International Journal of Pressure Vessels and Piping. 98 (2012) 95–101. https://doi.org/10.1016/j.ijpvp.2012.07.010.

[28] B. Bahrami Babamiri, A. Shahrjerdi, M. Bayat, Effect of geometrical imperfection on the thermomechanical behavior of functionally graded material rotating disk, J Braz. Soc. Mech. Sci. Eng. 42 (2020) 271. https://doi.org/10.1007/s40430-020-02360-z.

[29] M. Khorsand, Y. Tang, On the qualitative dynamics of rotating disks: Thermal shocks and structural integrity, International Journal of Pressure Vessels and Piping. 166 (2018) 35–47. https://doi.org/10.1016/j.ijpvp.2018.08.001.

[30] X.-L. Peng, X.-F. Li, Thermal stress in rotating functionally graded hollow circular disks, Composite Structures. 92 (2010) 1896–1904. https://doi.org/10.1016/j.compstruct.2010.01.008.

[31] S. Deka, A. Mallick, P.P. Behera, P. Thamburaja, Thermal stresses in a functionally graded rotating disk: An approximate closed form solution, Journal of Thermal Stresses. 44 (2021) 20–50. https://doi.org/10.1080/01495739.2020.1843377.

[32] V.R. Manthena, V.B. Srinivas, G.D. Kedar, Analytical solution of heat conduction of a multilayered annular disk and associated thermal deflection and thermal stresses, Journal of Thermal Stresses. 43 (2020) 563–578. https://doi.org/10.1080/01495739.2020.1735975.

[33] Y. Ootao, Y. Tanigawa, Transient Thermoelastic Analysis for a Multilayered Hollow Circular Disk with Piecewise Power Law Nonhomogeneity, Journal of Thermal Stresses. 35 (2012) 75–90. https://doi.org/10.1080/01495739.2012.637749.

[34] M.Z. Nejad, M.D. Kashkoli, Time-dependent thermo-creep analysis of rotating FGM thick-walled cylindrical pressure vessels under heat flux, International Journal of Engineering Science. 82 (2014) 222–237. https://doi.org/10.1016/j.ijengsci.2014.06.006.

[35] M.R. Abd-El-Salam, A.M. Abd-Alla, H.A. Hosham, A numerical solution of magneto-thermoelastic problem in non-homogeneous isotropic cylinder by the finite-difference method, Applied Mathematical Modelling. 31 (2007) 1662–1670. https://doi.org/10.1016/j.apm.2006.05.009.

[36] S.P. Pawar, K.C. Deshmukh, J. Verma, Thermal behavior of functionally graded solid sphere with nonuniform heat generation, Journal of Thermal Stresses. 40 (2017) 86–95. https://doi.org/10.1080/01495739.2016.1211928.

[37] B. Arnab, S.M.R. Islam, A.A. Khalak, A.M. Afsar, Finite Difference Solution to Thermoelastic Field in a Thin Circular FGM Disk with a Concentric Hole, Procedia Engineering. 90 (2014) 193–198. https://doi.org/10.1016/j.proeng.2014.11.836.

[38] Y.A. Cengel, Heat Transfer: A Practical Approach, Mcgraw-Hill, Boston, 2002.